Using Proximity and Quantized RSS for Sensor Localization in Wireless Networks *

Neal Patwari
npatwari@eecs.umich.edu

Alfred O. Hero III
hero@eecs.umich.edu

University of Michigan
Dept. of Electrical Engineering and Computer Science
1301 Beal Avenue
Ann Arbor, MI, USA

ABSTRACT

For wireless sensor networks, received signal strength (RSS) and proximity (also known as connectivity) measurements have been proposed as simple and inexpensive means to estimate range between devices and sensor location. While RSS measurements are recognized to suffer from errors due to the random nature of the fading channel, proximity measurements, ie., knowing only whether or not two devices are in communication range, are often discussed without considering that they are affected by the same fading channel. Proximity measurements are actually just a binary quantization of RSS measurements. We use the Cramér-Rao bound (CRB) to compare the minimal attainable variances of unbiased sensor location estimators for the cases of RSS and proximity measurements. For completeness, we also present the CRB for sensor localization with systems using K-level quantized RSS (QRSS) measurements, of which proximity measurements are the special case: $K = 2$. Examples are presented for the case of one unknown-location sensor, and for the case of a 5 by 5 grid of sensors. These examples show that lower bounds for standard deviation in proximity-based systems are, as a rule of thumb, about 50% higher than the bounds for RSS-based systems. Furthermore, results are presented which show how many bits of quantization are necessary for a QRSS-based system to nearly achieve the bounds of an unquantized RSS system.

Categories and Subject Descriptors

C.4 [**Performance of Systems**]: Performance attributes

General Terms

Performance

Keywords

Localization, wireless sensor networks, proximity, received signal strength, Cramér-Rao lower bound

1. INTRODUCTION

Emerging applications of wireless sensor networks will depend on automatic and accurate location of thousands of sensors. In environmental sensing applications such as water quality monitoring, precision agriculture, and indoor air quality monitoring, "sensing data without knowing the sensor location is meaningless"[22]. In addition, by helping reduce configuration requirements and device cost, estimation of sensor location in wireless sensor networks may enable applications such as inventory management [9], intrusion detection [15], traffic monitoring, and locating emergency workers in buildings. Finally, knowing the relative locations of sensors allows use of location-based addressing and routing protocols, which can improve network robustness and energy-efficiency [12].

Constrained by cost, energy, and low-configuration requirements, wireless sensor networks pose new challenges for location estimation. The literature reflects widespread interest in developing the technologies needed to achieve location estimation in wireless sensor networks [1][24][30][27][8][15][17][21].

Location accuracy requirements vary with the application. For applications as diverse as mentioned above, many different requirements exist. For high accuracy sensor location, measuring time-of-arrival (TOA) and angle-of-arrival are preferred. Ranging via TOA has been implemented with UWB [9], wideband CDMA [13], acoustics [16], and a combination of RF and ultrasound [10][26]. Range accuracy on the order of centimeters has been reported. However, TOA and AOA methods typically add to the size, cost and energy requirements of each device.

When low cost takes precedence in priority over accuracy, localization using RSS and proximity measurements are popular. Many receivers are equipt to measure the RSS of incoming packets for other purposes, such as automatic gain control or transmit power control. Proximity is just a binary variable which is one if a packet transmitted by

*This research was partially supported by a U. of Michigan Dept. of Electrical Engineering & Computer Science Graduate Fellowship and by ARO-DARPA MURI Grant #DAAD19-02-1-0262.

WSNA'03, September 19, 2003, San Diego, California, USA.

one device can be received by another device, and zero if not. Since messages necessarily pass between neighbors, there is no additional bandwidth required to measure RSS or proximity. In RSS, the measured received power and the known transmit power are used to determine the channel path loss. Although the path loss is also affected by unpredictable shadowing and frequency-selective fading, path loss is highly correlated with path length. Location estimation using RSS has been researched and simulated for wireless sensor networks in [18][28][3][14] and demonstrated in [21][20][2].

Proximity measurements simply report whether or not two devices are 'connected' or 'in-range'. However, the term 'in-range' may mislead readers to believe that proximity is purely a function of geometry - whether or not two devices are separated by less than a particular distance. In reality, proximity is determined by whether or not a receiver can demodulate and decode a packet sent by a transmitter. Given the received signal and noise powers, the successful reception of a packet is a random variable. Furthermore, the received signal power is a random variable due to the same channel fading effects mentioned for RSS above. Yet proximity carries considerable information regarding sensor location in a binary variable. Proximity has been used by numerous researchers for localization in ad hoc networks and wireless sensor networks [29][8][17][18][5][6].

Much past research has used simulation and experimentation to quantify how accurately location can be estimated using proximity measurements. Yet, to our knowledge, theoretical lower bounds on location estimation error have not been presented. In this paper, we derive the Cramér-Rao bound (CRB), which provides a lower bound on the variance for any unbiased location estimator. The CRB has been widely used to provide bounds for location estimation in sensor networks when the measurements are TOA and AOA [16][25], and when measurements are either TOA or RSS [19][20]. In this paper, we present the CRB for both proximity and K-level quantized received signal strength (QRSS) measurements. Comparing proximity and RSS bounds allows us to determine the performance loss associated with proximity as compared to the performance of RSS. Furthermore, since proximity measurements are just a binary quantization of RSS, we can use the K-level QRSS result to see how the performance improves as K is increased beyond 2. Finally, we can judge how many quantization levels in QRSS are needed to approach the performance of localization using RSS measurements.

2. MEASUREMENT MODELS

Wireless sensor networks are made up of peer-to-peer links between devices. Pair-wise measurements can be made from any of these links, but only a small fraction of devices have *a priori* coordinate knowledge. Thus measurements are made primarily between pairs of devices of which neither has known coordinates. We call devices with *a priori* coordinate knowledge 'reference devices' and those without 'blindfolded devices' since they cannot 'see' their location. Specifically, consider a network of m reference and n blindfolded devices. The device parameters are $\boldsymbol{\gamma} = [\mathbf{z}_1, \ldots, \mathbf{z}_{m+n}]$ where, for a 2-D system, $\mathbf{z}_i = [x_i, y_i]^T$. The relative location problem corresponds to the estimation of blindfolded device coordinates, $\boldsymbol{\theta} = [\boldsymbol{\theta}_x, \boldsymbol{\theta}_y]$,

$$\boldsymbol{\theta}_x = [x_1, \ldots, x_n], \quad \boldsymbol{\theta}_y = [y_1, \ldots, y_n] \tag{1}$$

given the known reference coordinates $[x_{n+1}, \ldots, x_{n+m}, y_{n+1}, \ldots, y_{n+m}]$, and pair-wise measurements $\{X_{i,j}\}$, where $X_{i,j}$ is a measurement between devices i and j.

To be general, we allow for the case when devices make incomplete observations, since the network may have limited link capacity. For example, the pairwise measurements might be made using a slotted ALOHA protocol. A centralized device which knows the packet transmission times of each device might decide not to use certain pairwise measurements which could have been tainted by multi-user interference (MUI). Let $H(i) = \{j : \text{device } j \text{ makes pair-wise observations with device } i\}$. By convention, a device cannot make a pair-wise observation with itself, so that $i \notin H(i)$. By symmetry, if $j \in H(i)$ then $i \in H(j)$.

2.1 Channel Fading Models

All of the types of measurements considered in this paper - RSS, K-level QRSS, and proximity - are subject to the deleterious effects of a fading channel. Received signal strength is attenuated by large scale path losses, frequency selective (a.k.a. small-scale) fading, and shadowing losses [11]. Large-scale path loss is the effect that we wish to measure - it is the deterministic reduction in power as a function of distance between the transmitter and receiver. Frequency selective fading is due to multipath - the multiple attenuated and time-delayed signals that add together at the receiver. At a particular frequency, each signal's time delay translates into a phase shift, and the sum of the multiple signals as a result adds either constructively or destructively. This fading is correlated over frequency. However, if RSS measurements are made at multiple frequencies spaced further than the correlation bandwidth of the channel, the correlation between the measurements is small, allowing the variance of the average RSS to be reduced. Note that many wireless sensors will be spread-spectrum, either direct-sequence or frequency-hopping spread-spectrum (DS-SS or FH-SS), and thus will be capable of averaging out frequency-selective fading.

Shadowing is the loss incurred as a signal passes through permanent obstructions (eg. buildings, walls, windows, and furniture) which are in the environment between the transmitter and receiver. For mostly stationary devices such as wireless sensors, shadowing losses cannot be countered by averaging over frequency. Some movement (eg. people, doors, chairs) can change the channel over time, allowing time-averaging to help reduce fading, but the majority of shadowing effects are constant over time. There is both experimental and theoretical evidence that these shadowing losses are well-modeled as log-normal random variables [7][11][23]. Although frequency-selective fading effects are typically not modeled as log-normal, we assume that the system designer has averaged enough so that their impact on the overall distribution of fading is not significant. Since this goal of this paper is to present the best performance possible, it is reasonable to make this assumption about the system design. As will be discussed in the next section, measurements of RSS in peer-to-peer networks in [21] and [20] do not violate the log-normal assumption.

Note that shadowing is not assumed to be an ergodic random variables – in fact, obstructions in the measured envi-

ronment that cause shadowing do not usually change over time. The CRB presented in this paper provides a lower bound on the ensemble variance over different random shadowing environments. If networks with the same relative device coordinates are implemented in many different places, the variances of any unbiased coordinate estimator will be lower bounded by the CRB presented in this paper.

2.2 RSS Measurements

In the RSS case, $X_{i,j} = P_{i,j}$ is the measured received power at device i transmitted by device j (in mW). We assume that $P_{i,j}$ is log-normal, thus the random variable $P_{i,j}(\text{dBm}) = 10\log_{10} P_{i,j}$ is Gaussian,

$$\begin{aligned} P_{i,j}(\text{dBm}) &\sim \mathcal{N}(\bar{P}_{i,j}(\text{dBm}), \sigma^2_{dB}) \\ \bar{P}_{ij}(\text{dBm}) &= \Pi_0(\text{dBm}) - 10n_p \log_{10}(d_{i,j}/\Delta_0) \end{aligned} \quad (2)$$

where $\bar{P}_{i,j}(\text{dBm})$ is the mean power in dBm, σ^2_{dB} is the variance of the shadowing, and $\Pi_0(\text{dBm})$ is the received power at the reference distance Δ_0. Typically $\Delta_0 = 1$ meter, and Π_0 is calculated from the free space path loss formula [23]. The path loss exponent n_p is a function of the environment. For particular environments, n_p may be known from prior measurements. Although we derive the CRB assuming n_p is known, the CRB could just as well be derived assuming that n_p is an unknown 'nuisance' parameter.

In [20], we verified the log-normal distribution assumption by making RSS measurements with a DS-SS transmitter and receiver in a network of 44 device locations (for a total of 946 pair-wise RSS measurements). We considered $P_{i,j}(\text{dBm}) - \bar{P}_{ij}(\text{dBm})$, ie., the attenuation of the channel that is attributable to frequency-selective fading and shadowing. The distribution of $P_{i,j}(\text{dBm}) - \bar{P}_{ij}(\text{dBm})$ is compared to the Gaussian distribution in a quantile-quantile plot in Fig. 1, which it matches well.

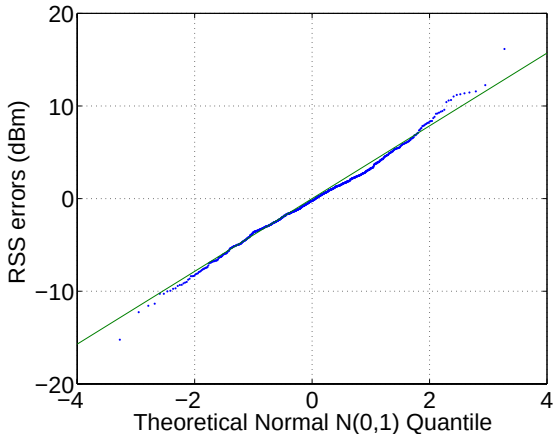

Figure 1: Quantile-quantile plot of $P_{i,j}(\text{dBm}) - \bar{P}_{i,j}(\text{dBm})$ for RSS data $(\cdots)$ measured in [20],compared with a Gaussian $\mathcal{N}(0,1)$ distribution. If data were perfectly Gaussian, they would match the solid line.

When discussing RSS measurements in this paper, we do not consider that there is a lower detection threshold for received power. This is done to distinguish RSS and proximity, which does have a detection threshold. For the examples presented in this paper, we assume that the distances between devices (or the transmit powers) are such that RSS can be measured between any pair of devices. A hybrid system was considered in [21], in which RSS measurements can fall below a detection threshold, and the out-of-range information is used in a location estimator.

2.3 Proximity Measurements

In the case of proximity measurements, $X_{i,j} = Q_{i,j}$ is equal to 1 if devices i and j are in range, and is 0 if not. As discussed in the introduction, 'in range' and 'out-of-range' are ambiguous, so we must define proximity clearly. In this paper, we define device i to be in-range of device j if the received power at j transmitted by i, $P_{i,j}$, falls below a power threshold P_1. Thus,

$$Q_{i,j} = \begin{cases} 1, & P_{i,j} \geq P_1 \\ 0, & P_{i,j} < P_1 \end{cases} \quad (3)$$

In reality, being in-range of another device is not a step function of received power. In a real system, two devices are considered in-range if one can correctly decode a packet transmitted by the other. An additional source of variation in proximity measurements is the randomness of packet errors given the received power level. Thus in reality, given received power $P_{i,j}$, proximity $Q_{i,j} \in \{0,1\}$ is a binary random variable, such that

$$\mathcal{P}[Q_{i,j} = 1 | P_{i,j}] = \mathcal{P}\left[\text{No Packet Error} | P_{i,j}\right] \quad (4)$$

where the probability of a packet error is a function of the type of signalling and forward error correction (FEC) used, packet length, and whether the receiver is coherent or non-coherent. If we used (4) to define proximity, all of these details of the transceiver implementation would be required in order to calculate the CRB. Instead, by using (3) we can present a bound that is independent of signaling, packet length, and receiver implementation. Since (3) removes some variability from the measurement model, the calculated CRB is conservative: it does in fact provide a lower bound for a proximity system.

Finally, we note that the assumption in (3) will not loosen the bound significantly for digital receivers in typical fading channels. For digital receivers, there is a large range of received powers for which the probability of packet error is very close to zero, and a large range of power for which the probability is very close to one. The range of power for which $P(E)$ is neither close to one or zero is small in comparison. Fig. 2 plots $\mathcal{P}[\text{No Packet Error}|P_{i,j}]$ from (4) for a packet of 200 bits and a coherent BPSK receiver without FEC. For comparison, Fig. 2 also plots the CDF of received power under a log-normal model with standard deviation of 8 dB, which is a typical value for indoor channels [23]. We can see that the variation caused by the fading channel is significantly more severe than that caused by the randomness of packet errors given the received power level.

Given the definition of proximity in (3) and the model for $P_{i,j}$ in (2), it can be shown that the probability mass

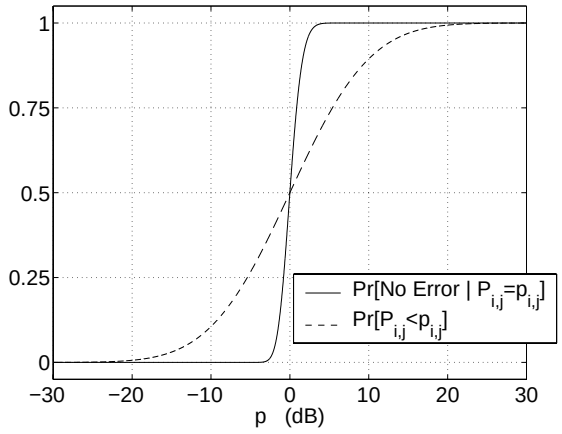

Figure 2: Two plots relating to the variation in proximity measurements: (- - - -) the CDF of $P_{i,j}$ in dB above $\bar{P}_{i,j}$, and (——) the probability of no packet error given $P_{i,j}$ in dB above P_{thr} (for a packet of 200 bits and a coherent BPSK receiver without FEC).

function of $Q_{i,j}$ given the coordinates of devices i and j is

$$\mathcal{P}[Q_{i,j} = s|\mathbf{z}_i, \mathbf{z}_j] = s + (-1)^s \Phi\left[g_{i,j}(1)\right], \quad (5)$$

$$g_{i,j}(s) = \sqrt{b} \ln \frac{\|\mathbf{z}_i - \mathbf{z}_j\|}{d_s} \quad (6)$$

$$b = \left(\frac{10 n_p}{\sigma_{dB} \log 10}\right)^2, \quad (7)$$

$$\|\mathbf{z}_i - \mathbf{z}_j\| = \sqrt{(x_i - x_j)^2 + (y_i - y_j)^2}, \quad (8)$$

where $s \in \{0, 1\}$, and d_s is the path length at which the mean received power is P_s, ie., the communication 'range'. Specifically, from (2),

$$d_s = \Delta_0 10^{\frac{\Pi_0(\text{dBm}) - P_s(\text{dBm})}{10 n_p}}. \quad (9)$$

The function $\Phi(x)$ is the CDF of a univariate zero-mean unit-variance Normal distribution.

2.4 Quantized RSS Measurements

As noted in the introduction, proximity measurements are just a binary quantization of RSS measurements. For more generality, we consider an arbitrary K-level quantized received signal strength (QRSS) system. For example, consider a transmitter which has the option of using a power amplifier (PA). The transmitter could send a packet twice - once using the PA, and once without. Assuming a stationary channel during the two measurements, one of three results are possible, essentially resulting in a single 3-level QRSS measurement.

Also, consider that real-world RSS measurements are always going to be quantized. If there are very many levels, then the effect of the quantization is minimal. However, if an A/D converter is used to quantize an analog measure of received power, the complexity of the A/D increases linearly with the number of levels. Determining the acceptable granularity of measured RSS will be valuable in minimizing receiver complexity.

Expanding on the model for proximity measurements, we define K levels numbered 0 through $K-1$. For a particular system, we define the threshold powers P_s, $s \in \{1, \ldots, K-1\}$ to be the minimum power in level s. Similarly, we define d_s to be the path length at which the mean received power is equal to P_s, as in (9). Thus, a measurement of $Q_{i,j} = s$ would occur if $P_{i,j} \in [P_s, P_{s+1})$. Similarly, $Q_{i,j} = s$ would occur if $\tilde{d}_{i,j} \in (d_{s+1}, d_s]$, where

$$\tilde{d}_{i,j} = \Delta_0 10^{\frac{\Pi_0(\text{dBm}) - P_{i,j}(\text{dBm})}{10 n_p}} \quad (10)$$

Since there is no lower bound for 'out-of-range' power (the lower bound of level $s = 0$), we define $P_0 = -\infty(\text{dBm})$. Similarly, since we would prefer not to define a maximum measured power (the upper bound of level $s = K-1$), we define $P_K = \infty(\text{dBm})$. Using (9), this implies that $d_0 = \infty$ and $d_K = 0$. Note P_s are increasing in s, but d_s are decreasing in s.

Now we can write the probability mass function of QRSS measurements,

$$\mathcal{P}[Q_{i,j} = s|\mathbf{z}_i, \mathbf{z}_j] = \Phi\left[g_{i,j}(s+1)\right] - \Phi\left[g_{i,j}(s)\right], \quad (11)$$

where $g_{i,j}(k)$ is given in (6) and we use the convention that for $0 < d < \infty$, $\ln \frac{d}{0} = \infty$ and that $\ln \frac{d}{\infty} = -\infty$.

3. CRB FOR LOCATION ESTIMATION

Let $\hat{x}_i$ and $\hat{y}_i$ be unbiased estimators of the coordinates of the ith device, x_i and y_i, and define the vector $\hat{\mathbf{z}}_i = [\hat{x}_i, \hat{y}_i]^T$. We define the location variance of these estimators to be σ_i^2,

$$\sigma_i^2 \triangleq \text{tr}\left\{\text{cov}_{\boldsymbol{\theta}}(\hat{\mathbf{z}}_i)\right\} = \text{Var}_{\boldsymbol{\theta}}(\hat{x}_i) + \text{Var}_{\boldsymbol{\theta}}(\hat{y}_i). \quad (12)$$

Then the Cramér-Rao bound asserts that,

$$\sigma_i^2 \geq \left(\left[\mathbf{F}_{xx} - \mathbf{F}_{xy}\mathbf{F}_{yy}^{-1}\mathbf{F}_{xy}^T\right]^{-1}\right)_{i,i} + \left(\left[\mathbf{F}_{yy} - \mathbf{F}_{xy}\mathbf{F}_{xx}^{-1}\mathbf{F}_{xy}^T\right]^{-1}\right)_{i,i}, \quad (13)$$

where the Fisher information matrix $\mathbf{F}$ is divided into sub-blocks due to the partition of the parameter vector $\boldsymbol{\theta}$ into $\boldsymbol{\theta}_x$ and $\boldsymbol{\theta}_y$,

$$\mathbf{F} = \begin{bmatrix} \mathbf{F}_{xx} & \mathbf{F}_{xy} \\ \mathbf{F}_{xy}^T & \mathbf{F}_{yy} \end{bmatrix}. \quad (14)$$

The specific form of each sub-block of $\mathbf{F}$ is shown below for the cases when measurements are QRSS or proximity measurements. For comparison, the CRB using RSS measurements was presented in [19][20].

3.1 CRB for QRSS Measurements

Using the framework presented in [20] and the models presented in Section 2, we derive in the Appendix that when measurements are K-level QRSS, the elements of the sub-blocks of $\mathbf{F}$ are given by,

$$\left[\mathbf{F}_{xx}\right]_{k,l} = \begin{cases} \frac{b}{2\pi} \sum_{i \in H(k)} h_{k,i} \frac{(x_k - x_i)^2}{\|\mathbf{z}_k - \mathbf{z}_i\|^4} & k = l \\ -\frac{b}{2\pi} I_{H(k)}(l) h_{k,l} \frac{(x_k - x_l)^2}{\|\mathbf{z}_k - \mathbf{z}_l\|^4} & k \neq l \end{cases}$$

$$\left[\mathbf{F}_{xy}\right]_{k,l} = \begin{cases} \frac{b}{2\pi} \sum_{i \in H(k)} h_{k,i} \frac{(x_k - x_i)(y_k - y_i)}{\|\mathbf{z}_k - \mathbf{z}_i\|^4} & k = l \\ -\frac{b}{2\pi} I_{H(k)}(l) h_{k,l} \frac{(x_k - x_l)(y_k - y_l)}{\|\mathbf{z}_k - \mathbf{z}_l\|^4} & k \neq l \end{cases}$$

$$\left[\mathbf{F}_{yy}\right]_{k,l} = \begin{cases} \frac{b}{2\pi} \sum_{i \in H(k)} h_{k,i} \frac{(y_k - y_i)^2}{\|\mathbf{z}_k - \mathbf{z}_i\|^4} & k = l \\ -\frac{b}{2\pi} I_{H(k)}(l) h_{k,l} \frac{(y_k - y_l)^2}{\|\mathbf{z}_k - \mathbf{z}_l\|^4} & k \neq l \end{cases}, \quad (15)$$

where b is given in (7), $I_{H(k)}(l)$ is the indicator function, 1 if $l \in H(k)$, or 0 if not, and $\{h_{i,j}\}$ are defined as,

$$h_{i,j} = \sum_{s=0}^{K-1} \frac{\left[\exp\left(-\frac{1}{2}g_{i,j}^2(s+1)\right) - \exp\left(-\frac{1}{2}g_{i,j}^2(s)\right)\right]^2}{\Phi\left(-g_{i,j}(s+1)\right) - \Phi\left(-g_{i,j}(s)\right)}. \quad (16)$$

Here, $g_{i,j}^2(s) = [g_{i,j}(s)]^2$ is defined in (6). Compared to the CRB for RSS measurements presented in [19][20], the terms of the Fisher information matrix are the same except for the the term $h_{i,j}$.

3.2 CRB for Proximity Measurements

Consider the particular case of $K = 2$, ie., proximity measurements. The CRB for the case of proximity measurements is the same as given in (13) through (15), but now, $h_{i,j}$ simplifies considerably. The resulting expression is given by,

$$h_{i,j} = \frac{\exp[-g_{i,j}^2(1)]}{\Phi\left[-g_{i,j}(1)\right]\left\{1 - \Phi\left[-g_{i,j}(1)\right]\right\}}. \quad (17)$$

The term $h_{i,j}$ has a maximum when $g_{i,j}(1) = 0$, which happens when devices are separated by approximately the threshold distance d_1. The selection of the threshold distances $\{d_s\}$ is explored further in the examples in the following sections.

4. EXAMPLE: SINGLE BLINDFOLDED DEVICE

Consider the network having blindfolded device 1 and reference devices $2 \ldots m+1$. This example has a single pair of unknowns (x_1, y_1), and is equivalent to the system model presented in [5] for proximity measurements. In addition, for RSS measurements, this example is equivalent to existing location systems [4].

For a simple example, consider the case when $m = 4$ reference devices are located in the corners of a 1 meter by 1 meter square area. We assume that the blindfolded device makes measurements with all four reference devices. Further, we assume the value of the parameter ratio, $\sigma_{dB}/n_p = 1.7$, which was calculated from measurements in [20]. For the case of RSS measurements, the lower bound for σ_1 is calculated from [20] and plotted as a function of blindfolded device location in Fig. 3(a). The minimum of the CRB for σ_1 for the case of RSS measurements is 0.27 m, and the average bound within the square is 0.305 m.

For proximity or QRSS measurements, the bound is a function of the threshold distances $\{d_s\}$. For a system using proximity measurements, designers can select the threshold distance d_1 by changing either the sensitivity of the receiver, or the transmit power level. A QRSS system additionally must set d_s for $s = 2 \ldots K-1$, which can be done either by design of the A/D in the receiver, or by design of the power amplifier transmit power levels. Other system considerations, for example, network connectivity and energy efficiency, must also be considered when setting these parameters. In this paper, in order to present a universal lower bound, we set d_1 and $d_2 \ldots d_{K-1}$ as the distances that minimize the lower bound σ_1. Specifically, we minimize this bound for the case when the blindfolded device is located in the center of the square area, ie., $\mathbf{z}_1 = [0.5, 0.5]^T$ m.

4.1 Proximity

Since the blindfolded device is located equidistant from all of the reference devices, the analytical expression for the CRB simplifies considerably. In particular, the CRB is minimized when d_1 is equal to the distance between the blindfolded device and any of the reference devices, ie., $d_1 = 1/\sqrt{2}$ m. In this case, the CRB is given by,

$$\sigma_i^2 \geq \frac{\pi}{4}\left(\frac{\sigma_{dB}\log 10}{10 n_p}\right)^2. \quad (18)$$

For $\sigma_{dB}/n_p = 1.7$, the bound on the standard deviation σ_i is 0.3477 m. This is verified graphically in Fig. 3(b), which plots the bound on the standard deviation of unbiased location estimates as a function of the location of the blindfolded device, while the design parameter $d_1 = 1/\sqrt{2}$ m is kept constant. Furthermore, the average standard deviation bound within the square is 0.45 m. Note that the average standard deviation bound using proximity measurements is 48% worse as compared to the bound obtained using RSS measurements.

4.2 Three-Level QRSS

Next we consider the performance of the system in the case of $K = 3$ QRSS measurements. Again, we optimize the system to minimize the CRB when the blindfolded device is located at $\mathbf{z}_1 = [0.5, 0.5]^T$ m. It can be shown that the CRB as a function of the two threshold distances, d_1 and d_2, is given by,

$$\sigma_i^2 \geq \frac{2}{f_{1,1}} \quad (19)$$

$$f_{1,1} = \frac{2b}{\pi}\left\{\frac{\exp\left[-b\ln^2\frac{d_a}{d_1}\right]}{\Phi\left(-\sqrt{b}\ln\frac{d_a}{d_1}\right)} + \frac{\exp\left[-b\ln^2\frac{d_a}{d_2}\right]}{\Phi\left(-\sqrt{b}\ln\frac{d_a}{d_2}\right)} + \frac{\left[\exp\left(-\frac{b}{2}\ln^2\frac{d_a}{d_2}\right) - \exp\left(-\frac{b}{2}\ln^2\frac{d_a}{d_1}\right)\right]^2}{\Phi\left(-\sqrt{b}\ln\frac{d_a}{d_2}\right) - \Phi\left(-\sqrt{b}\ln\frac{d_a}{d_1}\right)}\right\}$$

where d_a is the distance between the blindfolded device and any reference device, ie., $d_a = 1/\sqrt{2}$ m. The term $f_{1,1}$ is equal to $\mathbf{F}_{Qxx}$, ie., the Fisher information for the x-coordinate. Note the notation $\ln^2 x$ is used to indicate $(\ln x)^2$. As a result of (19), we must select d_1 and d_2 to maximize $f_{1,1}$. For a range of d_1 and d_2, the Fisher information $f_{1,1}$ is plotted in Fig. 4.

For three cases, the three-level QRSS Fisher information $f_{1,1}$ reverts to the two-level proximity Fisher information. These cases are (1) when $d_1 = d_2$, (2) when d_1 is very large, and (3) when d_2 is very small. Intuitively, we understand in any of these three cases, we effectively have only two levels, and the system reverts to a proximity system. Fig. 4 shows this graphically. The value of $f_{1,1}$ along the diagonal $d_1 = d_2$ can be seen to be the same as $f_{1,1}$ along the horizontal line at the lowest d_2, and along the vertical line at the highest d_1.

The maximum of $f_{1,1}$ occurs for $d_1 = 0.90$ m and $d_2 = 0.56$ m. For these two parameters, the bound on the standard deviation σ_i is 0.3076 m when the blindfolded device is at $\mathbf{z}_1 = [0.5, 0.5]^T$ m. The CRB as a function of blindfolded device location is plotted in Fig. 3(c). Furthermore, the average standard deviation bound within the square is 0.37 m.

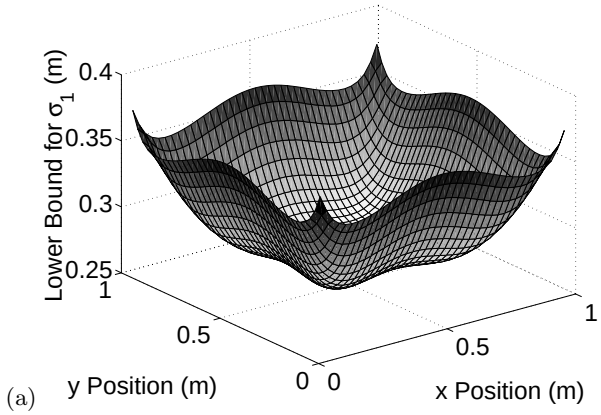

(a)

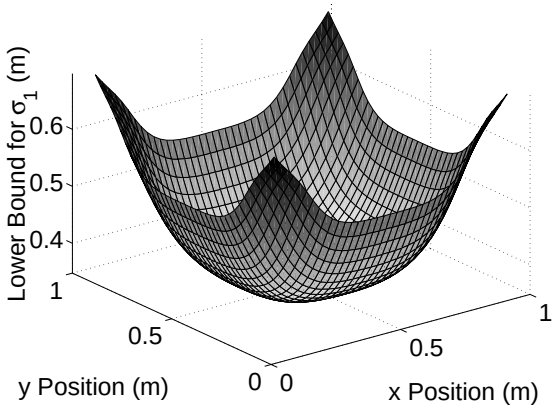

(b)

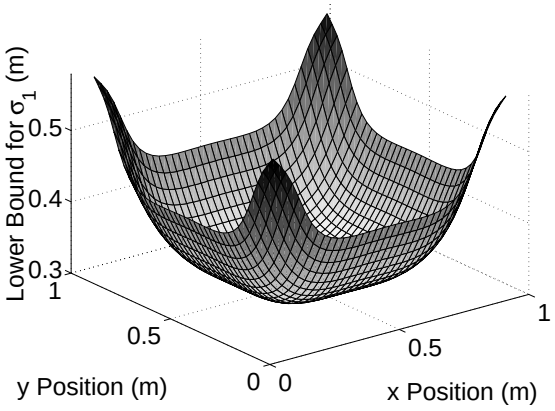

(c)

Figure 3: Lower bound for σ_1 (m) for the single blindfolded device system vs. the coordinates of the blindfolded device, in a channel with $\sigma_{dB}/n = 1.7$, for (a) RSS, (b) proximity with $d_1 = 1/\sqrt{2}$ m and (c) 3-level QRSS with $d_1 = 0.90$ m and $d_2 = 0.56$ m.

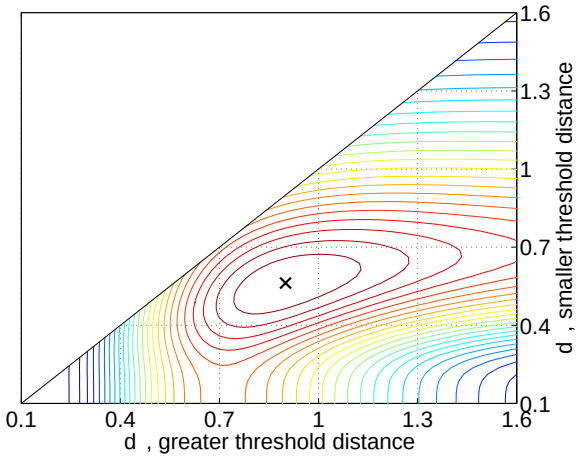

Figure 4: The Fisher information $f_{1,1}$ for the case of 3-level QRSS when a single blindfolded device is located in the center of a 1m by 1m square with reference devices in each corner. The FIM is plotted as a function of the two thresholds, d_2 and d_1, which separate the three QRSS regions. The maximum of $f_{1,1}$ (x) is at $d_1 = 0.90$ m and $d_2 = 0.56$ m. Since $d_2 \leq d_1$, only half of the plot is shown.

Note that in any of the three cases presented in this section, the CRB scales with the size of the system. If instead the square area had sides of length r, and the threshold distances d_s were scaled by r, then the bound on σ_i would also be scaled by r.

5. EXAMPLE: DEVICES IN A 5 BY 5 GRID

The previous single-blindfolded device example only tells part of the story, since most localization research in wireless networks has considered networks comprised of many blindfolded devices [17][18][29][8][26]. As more blindfolded devices in a network make peer-to-peer measurements with other devices (either blindfolded or reference), the location variance bounds decrease across the entire network, regardless of the type of measurements [20]. We will show the relative performance of RSS, QRSS, and proximity measurements in a dense sensor network in the following example.

In this example, devices form a 5 device by 5 device grid in a 1 by 1 meter square area. As before, there are 4 reference devices, one at each corner. The spacing between adjacent devices is 0.25 meters. There are a total of $5 \cdot 5 = 25$ devices, with $25 - 4 = 21$ blindfolded devices. The channel is again assumed to have $\sigma_{dB}/n = 1.7$, and each device is assumed to make measurements with all other devices.

Here, we chose to optimize the proximity and QRSS thresholds in order to optimize $\bar{\sigma}$, the average standard deviation of the 21 blindfolded devices,

$$\bar{\sigma} = \frac{1}{21} \sum_i \sigma_i \tag{20}$$

5.1 Proximity and 3-Level QRSS

For proximity measurements with this geometry of devices, we find by testing a range of d_1 that the lowest average standard deviation bound across the 21 blindfolded

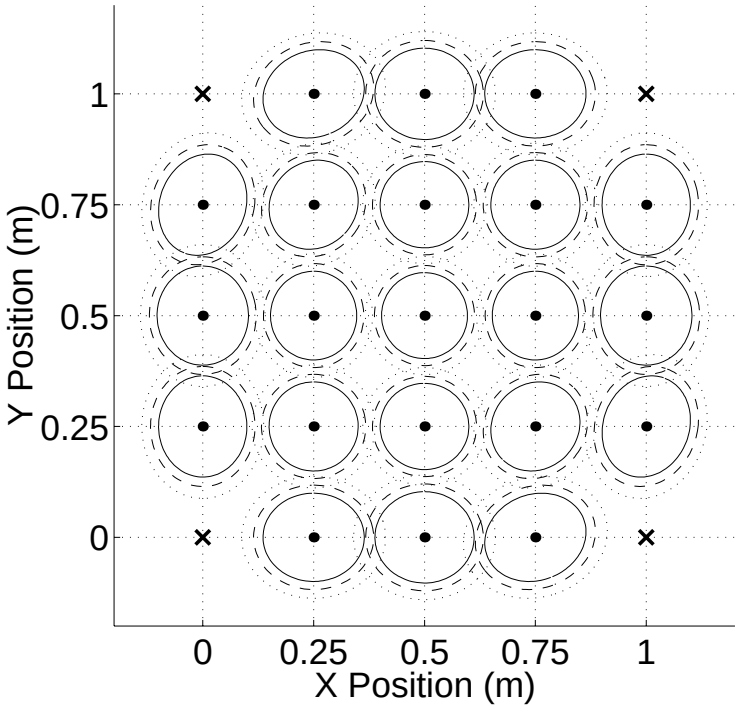

Figure 5: The lower bound on the 1-σ uncertainty ellipses in the 5 by 5 grid example when measurements are RSS (——), 3-level QRSS (- - - -), or proximity (· · · · · ·). Blindfolded devices (•) and reference devices (×) are located in a 1 by 1 m area.

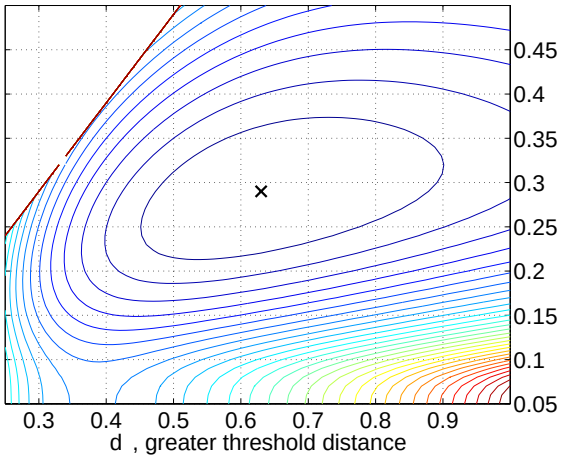

Figure 6: The lower bound on average standard deviation across all 21 blindfolded devices, as a function of the threshold distances d_1 and d_2, for the case of 3-level QRSS in the grid example. The minimum bound (X) is 0.1154 m, at the values $d_1 = 0.63$ m and $d_2 = 0.29$ m.

devices occurs at $d_1 = 0.38$ m. This threshold is used to calculate and plot the proximity location variance bound for each device in Fig. 5.

For 3-level QRSS, we calculate the CRB for a range of $0.25 \leq d_1 \leq 1$ m and $0 \leq d_2 \leq 0.5$ m (at increments of 0.01 m), as shown in Fig. 6. The minimum bound for $\bar{\sigma}$, given by (20), is found at the values $d_1 = 0.63$ m and $d_2 = 0.29$ m. These thresholds are used to calculate and plot the 3-level QRSS location variance bound for each device in Fig. 5.

Using these optimum threshold parameters, the lower bound for $\bar{\sigma}$ (20) is 0.115 m and 0.146 m, in the case of 3-level QRSS and proximity measurements, respectively. For RSS measurements, for comparison, $\bar{\sigma}$ =0.093 m. The bound for the proximity case is about 57% higher than the bound for the RSS case. The results for individual blindfolded devices are shown graphically by plotting the 1-standard-deviation uncertainty ellipse for each device in Fig. 5, for the cases of RSS, 3-level QRSS, and proximity measurements.

5.2 Quantized RSS Beyond 3 Levels

In this section we present results which quantify the decrease in the CRB as the number of quantization levels K increases. For this analysis, we continue to use the 5 by 5 grid of devices in a 1 by 1 m square area. From the previous section, we know the results for the cases of $K = 2$ (proximity measurements), $K = 3$ QRSS measurements, and the case of RSS measurements, which should match the asymptotic performance of QRSS as $K \to \infty$.

For a particular K, we should ideally find the $K-1$ thresholds $\{P_s\}_{s=1\ldots K-1}$ which minimize the bound on $\bar{\sigma}$. How-

ever, as K becomes large, finding a minimum in this $K-1$ dimensional space becomes more and more difficult. In addition, in a real low-cost implementation, the quantization of RSS is unlikely to be non-uniform. Specifically, RSS is often quantized on a log scale with a constant granularity in (dB). Thus it is reasonable to limit the search space to two parameters: the mean of P_s, ie. $\bar{P} = \frac{1}{K-1}\sum_{s=1}^{K-1} P_s$, and $\Delta P \triangleq P_{s+1} - P_s, \forall s = 1 \ldots K-2$. Equivalently, we can use the geometric mean of d_s, ie. $\bar{d} \triangleq \left(\prod_{s=1}^{K-1} d_s\right)^{1/(K-1)}$, and the parameter d_{ratio}, defined as $d_s/d_{s+1}, \forall s = 1 \ldots K-2$.

For these two parameters over wide ranges, we calculate the CRB for K-level QRSS. At each K, we find the $\bar{d}$ and d_{ratio} which minimize the bound for $\bar{\sigma}$. We repeat this search for each K, for $K = 4 \ldots 10$. The minimum bound for $\bar{\sigma}$ is plotted as a function of K in Fig. 7. Also shown in Fig. 7 is the RSS result for the same example, which gives the asymptotic limit for QRSS. The results show that for $K \geq 5$, the QRSS bound is within 10% of the bound for RSS. Thus, K-level QRSS rapidly approaches the limits of RSS as K increases. Interestingly, the value of $\bar{d}$ which minimizes the bound is approximately constant between 0.44 and 0.45 m for $K > 3$. Thus for a particular geometry of devices, there may be a rule-of-thumb for the selection of $\bar{d}$ (or equivalently $\bar{P}$) regardless of the value of K.

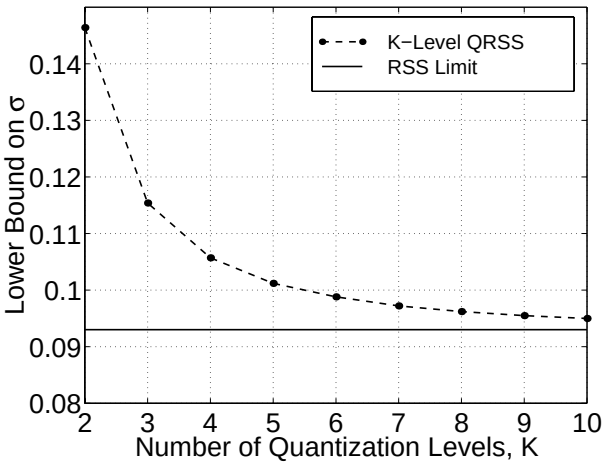

Figure 7: The lower bound on average standard deviation across all 21 blindfolded devices, as a function of the number of quantization levels K, for K-level QRSS in the 5 by 5 grid example.

6. SIMULATION: ACHIEVING THE BOUND

While the CRB does in fact provide a lower bound, we have not proven that it is tight. That is, we do not know if it is possible for any unbiased location estimator achieve the lower bound with equality. Further analytical research will be valuable in this regard. However, if we consider particular location estimators, we can determine their performance via simulation, and then compare the results to the CRB. In this section, we consider the performance of the bias-corrected MLE in the case when measurements are RSS [19][20],

$$\hat{\boldsymbol{\theta}}_R = \arg\min_{\{\mathbf{z}_i\}} \sum_{i=1}^{m+n} \sum_{j \in H(i), j<i} \left(\ln \frac{\tilde{d}_{i,j}^2 / C^2}{\|\mathbf{z}_i - \mathbf{z}_j\|^2} \right)^2 \qquad (21)$$

where $\tilde{d}_{i,j}$ is given in (10), and the factor C is used to counter the tendency of $\tilde{d}_{i,j}$ to overestimate the range between devices i and j. The value of C is given by

$$C = \exp\left[\frac{1}{2} \left(\frac{\ln 10}{10} \frac{\sigma_{dB}}{n_p} \right)^2 \right]. \qquad (22)$$

For this simulation, we use the 5 by 5 grid of devices, as described in the previous section. We run 500 trials. In each trial, we first generate the RSS between each pair of devices, based on the distribution of (2). Here, we use the parameters $n = 2.30$ and $\sigma_{dB} = 3.92$ dB, which were reported from measurements in [20]. Next, a conjugate gradient algorithm finds the minimum in (21), and the coordinate estimates are saved. After all trials are complete, we calculate the mean and covariance of the saved coordinate estimates. The one standard deviation (1-σ) uncertainty ellipses are calculating using the covariance of the vector $[\hat{x}_i, \hat{y}_i]^T$, for all $i = 1 \ldots 21$. The means and the 1-σ uncertainty ellipses are plotted in Fig. 8 with triangles and solid lines, respectively. For comparison, the true device locations and the Cramér-Rao lower bounds on the 1-σ uncertainty ellipses are plotted in Fig. 8 with circles and dotted lines, respectively.

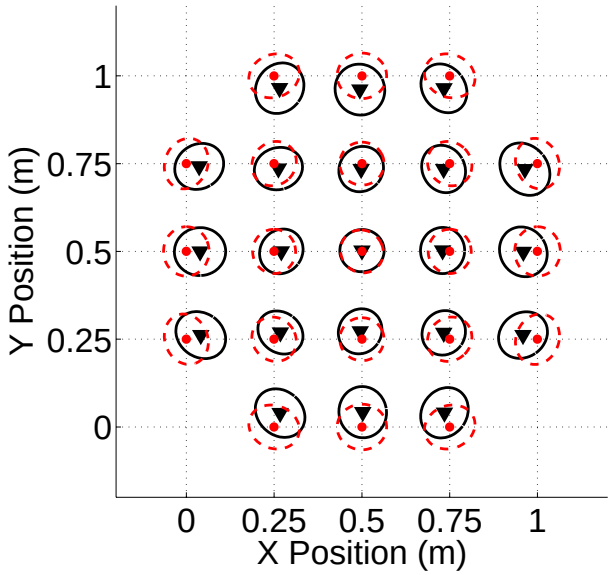

Figure 8: The simulated mean (▼) and 1-σ uncertainty ellipses (——) of the bias-reduced MLE in Eq. 21, and the true device locations (•) and CRB for the 1-σ uncertainty ellipses (- - - -), in the case of RSS measurements and the 5 by 5 grid of devices.

The simulation results show that the estimator is in fact biased, but that the estimator variances are very close to the bound. The bias of the estimator was implied by previous results [20] which showed that the bias-reduced MLE in the case of RSS measurements tended to pull estimates closer to the center of the square. However, the devices close to the center show very little bias. For these devices, the simulation shows uncertainty ellipses that are indistinguishable from the bounds. In addition, we note the similarity in the orientations of the minor and major axes of the uncertainty ellipses. Furthermore, if many of these 1m by 1m square areas were placed next to each other in a larger-scale im-

plementation, we would expect the biases at the edges to cancel. In that case, we expect that the estimator in (21) will be nearly unbiased, and thus the CRB will in fact provide its lower bound.

Comparison of particular proximity and QRSS location estimators to the CRB is beyond the scope of this paper. We note that initial results show that the MLE in the case of proximity measurements has a likelihood function which suffers from multiple local maxima, making global maximization difficult.

7. CONCLUSION

This paper has presented a variety of analytical results to aid in the design of sensor localization systems based on RSS, quantized RSS, or proximity measurements between sensors. Since low-cost is a key objective in the design of these wireless sensors, it is important to meet the design goals with the least device complexity. We have shown that variance bounds for unbiased location estimators using proximity measurements are significantly higher than for those using RSS measurements. In the single blindfolded device example, averaged over device location, the standard deviation bound for proximity measurements was 48% worse than that for RSS measurements. In a grid of devices, the proximity measurements had an average standard deviation bound about 57% worse than that of RSS measurements. Furthermore, since the area of uncertainty is proportional to the variance, rather than standard deviation, these differences are even more significant. However, we have shown that K-level QRSS can perform approximately as well as RSS for even low values of K. A system with just 3 bits of quantization ($K = 8$) may be enough in cases.

In order to deploy localization systems based on proximity or QRSS, future work must be done to explore the performance of particular location estimators which use quantized RSS or proximity measurements. Since perfectly unbiased location estimators seem unlikely when using proximity or QRSS measurements, it will likely require significant research to develop estimators with minimal bias for a wide variety of device geometries. These nearly unbiased estimators can then be compared to the bounds presented here in order to determine how much they might be improved, or if they do not need to be improved. Furthermore, it will be important to determine the sensitivity of location estimation to imperfect knowledge of the channel and threshold parameters. Finally, these bounds can, and should, be verified using multiple sets of channel measurements from networks of wireless sensors deployed in various environments.

8. REFERENCES

[1] J. Albowicz, A. Chen, and L. Zhang. Recursive position estimation in sensor networks. In *IEEE Int. Conf. on Network Protocols*, pages 35–41, Nov. 2001.

[2] P. Bahl and V. N. Padmanabhan. RADAR: an in-building RF-based user location and tracking system. In *IEEE INFOCOM 2000*, pages 775–784, 2000.

[3] P. Bergamo and G. Mazzini. Localization in sensor networks with fading and mobility. In *IEEE PIMRC*, pages 750–754, Sept. 2002.

[4] J. E. Berube. Personal security system with weighted receiver locations, April 1999. U.S. Patent 5,898,397. Detection Systems, Inc.

[5] N. Bulusu, J. Heidemann, and D. Estrin. GPS-less low cost outdoor localization for very small devices. *IEEE Personal Comm.*, 5(5):28–34, Oct. 2000.

[6] N. Bulusu, J. Heidemann, and D. Estrin. Adaptive beacon placement. In *Int. Conf. on Distributed Computing Systems*, pages 489–498, Apr 2001.

[7] A. J. Coulson, A. G. Williamson, and R. G. Vaughan. A statistical basis for lognormal shadowing effects in multipath fading channels. *IEEE Trans. on Veh. Tech.*, 46(4):494–502, April 1998.

[8] L. Doherty, K. S. J. pister, and L. E. Ghaoui. Convex position estimation in wireless sensor networks. In *IEEE INFOCOM*, volume 3, pages 1655 –1663, 2001.

[9] R. Fleming and C. Kushner. Low-power, miniature, distributed position location and communication devices using ultra-wideband, nonsinusoidal communication technology. Technical report, Aetherwire Inc., Semi-Annual Technical Report, ARPA Contract J-FBI-94-058, July 1995.

[10] L. Girod, V. Bychkovskiy, J. Elson, and D. Estrin. Locating tiny sensors in time and space: a case study. In *IEEE Int. Conf. on Computer Design*, pages 214–219, 2002.

[11] H. Hashemi. The indoor radio propagation channel. *Proceedings of the IEEE*, 81(7):943–968, July 1993.

[12] Y.-B. Ko and N. H. Vaidya. Location-aided routing (LAR) for mobile ad-hoc networks. In *ACM / IEEE MOBICOM '98*, Oct. 1998.

[13] D. D. McCrady, L. Doyle, H. Forstrom, T. Dempsy, and M. Martorana. Mobile ranging with low accuracy clocks. *IEEE Trans. on Microwave Theory and Techniques*, 48(6):951–957, June 2000.

[14] F. Mondinelli and Z. M. K. Vajna. Self localizing sensor network architectures. In *IEEE Instr. & Measurement Tech. Conf.*, volume 1, pages 823–828, May 2002.

[15] R. L. Moses, D. Krishnamurthy, and R. Patterson. An auto-calibration method for unattended ground sensors. In *ICASSP*, volume 3, pages 2941–2944, May 2002.

[16] R. L. Moses, D. Krishnamurthy, and R. Patterson. A self-localization method for wireless sensor networks. *EURASIP Journal on Applied Sig. Proc.*, (4):348–358, Mar. 2003.

[17] R. Nagpal, H. Shrobe, and J. Bachrach. Organizing a global coordinate system from local information on an ad hoc sensor network. In *2nd Intl. Workshop on Inform. Proc. in Sensor Networks*, April 2003.

[18] D. Niculescu and B. Nath. Ad hoc positioning system. In *IEEE Globecom 2001*, volume 5, pages 2926 –2931, April 2001.

[19] N. Patwari and A. O. Hero III. Location estimation accuracy in wireless sensor networks. In *Asilomar Conf. on Signals and Systems*, Nov. 2002.

[20] N. Patwari, A. O. Hero III, M. Perkins, N. Correal, and R. J. O'Dea. Relative location estimation in wireless sensor networks. *IEEE Trans. on Sig. Proc. Special Issue on Signal Processing in Networking*, 51(8):2137–2148, Aug. 2003.

[21] N. Patwari, R. J. O'Dea, and Y. Wang. Relative location in wireless networks. In *IEEE VTC*, volume 2, pages 1149–1153, May 2001.

[22] J. M. Rabaey, M. J. Ammer, J. L. da Silva, Jr., D. Patel, and S. Roundy. Picorodio supports ad hoc ultra-low power wireless networking. *IEEE Computer*, 33(7):42–48, July 2000.

[23] T. S. Rappaport. *Wireless Communications: Principles and Practice*. Prentice-Hall Inc., New Jersey, 1996.

[24] C. Savarese, J. M. Rabaey, and J. Beutel. Locationing in distributed ad-hoc wireless sensor networks. In *ICASSP*, pages 2037–2040, May 2001.

[25] A. Savvides, W. Garber, S. Adlakha, R. Moses, and M. B. Srivastava. On the error characteristics of multihop node localization in ad-hoc sensor netwoks. In *2nd Intl. Workshop on Inform. Proc. in Sensor Networks*, April 2003.

[26] A. Savvides, C.-C. Han, and M. B. Srivastava. Dynamic fine-grained localization in ad-hoc networks of sensors. In *IEEE Mobicom*, July 2001.

[27] A. Savvides, H. Park, and M. B. Srivastava. The bits and flops of the n-hop multilateration primitive for node localization problems. In *Intl. Workshop on Sensor Nets. & Apps.*, pages 112–121, Sept. 2002.

[28] S. Slijepcevic, S. Megerian, and M. Potkonjak. Location errors in wireless embedded sensor networks: Sources, models, and effects on applications. *ACM Sigmobile Mobile Comp. & Commun. Review*, 6(3):67–78, July 2002.

[29] N. Sundaram and P. Ramanathan. Connectivity based location estimation scheme for wireless ad hoc networks. In *IEEE Globecom 2002*, volume 1, pages 143–147, Nov. 2002.

[30] S. Čapkun, M. Hamdi, and J.-P. Hubaux. GPS-free positioning in mobile ad-hoc networks. In 34^{th} *IEEE Hawaii Int. Conf. on System Sciences (HICSS-34)*, Jan. 2001.

APPENDIX

A. DERIVATION OF CRB

In [20], the CRB for any self-calibration estimator was shown to be a function of the expected value of the second partial derivatives of the terms $\{l_{i,j}\}$,

$$l_{i,j} = \log \mathcal{P}[Q_{i,j}|\mathbf{z}_i, \mathbf{z}_j]. \tag{23}$$

The first partial derivatives of $l_{i,j}$ with respect to x_i are

$$\frac{\partial}{\partial x_i} l_{i,j} = \frac{\frac{\partial}{\partial x_i}\mathcal{P}[Q_{i,j}|\mathbf{z}_i, \mathbf{z}_j]}{\mathcal{P}[Q_{i,j}|\mathbf{z}_i, \mathbf{z}_j]}.$$

Similarly,

$$\frac{\partial^2}{\partial x_i^2} l_{i,j} = \frac{\frac{\partial^2}{\partial x_i^2}\mathcal{P}[Q_{i,j}|\mathbf{z}_i, \mathbf{z}_j]}{\mathcal{P}[Q_{i,j}|\mathbf{z}_i, \mathbf{z}_j]} - \left(\frac{\frac{\partial}{\partial x_i}\mathcal{P}[Q_{i,j}|\mathbf{z}_i, \mathbf{z}_j]}{\mathcal{P}[Q_{i,j}|\mathbf{z}_i, \mathbf{z}_j]}\right)^2.$$

Thus,

$$\begin{aligned} -\mathrm{E}\left[\frac{\partial^2}{\partial x_i^2} l_{i,j}\right] &= -\sum_{s=0}^{K-1} \frac{\partial^2}{\partial x_i^2}\mathcal{P}[Q_{i,j} = s|\mathbf{z}_i, \mathbf{z}_j] \\ &\quad + \sum_{s=0}^{K-1} \frac{\left(\frac{\partial}{\partial x_i}\mathcal{P}[Q_{i,j} = s|\mathbf{z}_i, \mathbf{z}_j]\right)^2}{\mathcal{P}[Q_{i,j} = s|\mathbf{z}_i, \mathbf{z}_j]}. \end{aligned} \tag{24}$$

The first sum is a telescoping sum of $\frac{\partial^2}{\partial x_i^2}\Phi[\cdot]$ terms,

$$\begin{aligned} &\sum_{s=0}^{K-1} \frac{\partial^2}{\partial x_i^2}\mathcal{P}[Q_{i,j} = s|\mathbf{z}_i, \mathbf{z}_j] = \\ &= \sum_{s=0}^{K-1} \frac{\partial^2}{\partial x_i^2}\Phi\left[g_{i,j}(s+1)\right] - \sum_{s=0}^{K-1} \frac{\partial^2}{\partial x_i^2}\Phi\left[g_{i,j}(s)\right] \\ &= \frac{\partial^2}{\partial x_i^2}\Phi\left[g_{i,j}(K)\right] - \frac{\partial^2}{\partial x_i^2}\Phi\left[g_{i,j}(0)\right] = 0. \end{aligned} \tag{25}$$

To further evaluate (24), we note that

$$\begin{aligned} &\frac{\partial}{\partial x_i}\mathcal{P}[Q_{i,j} = s|\mathbf{z}_i, \mathbf{z}_j] = \frac{\sqrt{b}}{\sqrt{2\pi}} \frac{x_i - x_j}{\|\mathbf{z}_i - \mathbf{z}_j\|^2} \\ &\left[\exp\left(-\frac{b}{2}\ln^2\frac{\|\mathbf{z}_i - \mathbf{z}_j\|}{d_{s+1}}\right) - \exp\left(-\frac{b}{2}\ln^2\frac{\|\mathbf{z}_i - \mathbf{z}_j\|}{d_{s+1}}\right)\right]. \end{aligned} \tag{26}$$

As a result of (25) and (26), (24) simplifies to

$$-\mathrm{E}\left[\frac{\partial^2}{\partial x_i^2} l_{i,j}\right] = \frac{b}{2\pi}\frac{(x_i - x_j)^2}{\|\mathbf{z}_i - \mathbf{z}_j\|^4} h_{i,j}, \tag{27}$$

where $h_{i,j}$ takes the form of (16). The terms depending on other second partial derivatives are very similar to (27).